Modeling Approach for Superconducting AC Windings: Case Study on Axial Flux PM Machines

Modeling Approach for Superconducting AC Windings: Case Study on Axial Flux PM Machines

Inês S. P. Peixoto, *Student Member, IEEE*
Politecnico di Torino
Dipartimento Energia
Torino, Italy
ines.peixoto@polito.it

Silvio Vaschetto, *Senior Member, IEEE*
Politecnico di Torino
Dipartimento Energia
Torino, Italy
silvio.vaschetto@polito.it

João F. P. Fernandes, *Member, IEEE*
IDMEC, Instituto Superior Técnico
University of Lisbon
Lisbon, Portugal
joao.f.p.fernandes@tecnico.ulisboa.pt

Paulo J. da Costa Branco, *Member, IEEE*
IDMEC, Instituto Superior Técnico
University of Lisbon
Lisbon, Portugal
pbranco@tecnico.ulisboa.pt

Alberto Tenconi, *Senior Member, IEEE*
Politecnico di Torino
Dipartimento Energia
Torino, Italy
alberto.tenconi@polito.it

Andrea Cavagnino, *Fellow, IEEE*
Politecnico di Torino
Dipartimento Energia
Torino, Italy
andrea.cavagnino@polito.it

***Abstract*— This paper aims to analyze the modeling of superconducting tapes when used for the realization of AC windings in rotating electrical machines. The model is based on literature formulations that describe the non-linear resistivity of superconducting materials, including the effects of external AC magnetic fields. An axial flux permanent magnet machine is considered as case study for applying the provided formulations. The 3D FEM machine model is solved considering both a conventional copper stator winding and superconducting counterpart, with the aim to verify the equivalence of these two winding solutions. Then, a 2D modeling approach of a single-slot is proposed for time-efficient investigations of the superconductor's behavior in the presence of the slot leakage flux.**

Keywords—Superconducting AC windings, cryogenic electrical machines, finite element analyses, high-temperature superconductors, T-A formulation.

I. Introduction

The enhancement of efficiency and torque density in electric machines are of paramount importance to fulfill the ambitious targets for reducing emissions and guarantee sustainability in transport, industry, and energy generation. Several works in the literature show that electric machines equipped with High-Temperature Superconductors (HTS), operated at temperatures between 35K to 120K, have the potential to outperform their conventional counterparts with copper windings [1]. In fact, in DC conditions, superconducting tapes and cables can present almost zero ohmic loss, thus improving the machine efficiency [2]. Moreover, their high current density capability can lead to a significant reduction in the machine size and volume, this being especially compelling when offshore applications or aviation are considered [3], [4].

Electrical machines employing superconductors (SCs) can be constructed either partially or fully superconducting. In the first case, the rotor or the stator have a conventional excitation (i.e. copper or permanent magnets), while in the second case the machine is fully excited by SCs. Since to keep the superconducting state requires cryogenic temperatures, constructing electrical machines with rotating cryostats becomes quite challenging. Consequently, the use of the SCs and the cryogenic cooling system to the stator side only would be highly advantageous from a construction and maintenance perspective.

In AC electrical machines, this means having a superconducting stator winding carrying AC currents. However, under AC regime, SCs can experience significant losses due to the presence of a time-varying magnetic field and currents that affect the SC itself. These losses can overheat the SC to a temperature higher than critical temperature (T_c) of the superconducting material, with the possibility of quenching – i.e., the sudden loss of superconductivity, and the consequent increase of resistivity [1]. For this reason, the application of SCs for AC stator windings of rotating electrical machines is still an open research field [5]-[8].

To limit the negative effect of the AC magnetic field, the winding can be shielded by positioning the conductors inside slots. Additionally, during the design stage of superconducting AC electrical machines, Finite Element Method (FEM) models are indispensable to evaluate different positioning of the SCs in the slot to minimize the AC magnetic field that affects the SCs, the related losses and the quench/damage risk. The literature reports various formulations to model superconductors. However, the intrinsic non-linear behavior of SCs together with their '*lilliputian*' geometrical dimensions, make the modeling and simulation of AC superconducting electrical machines very time consuming and computationally demanding. This complexity is further exacerbated if 3D FEM models must be used due to the three-dimensional nature of the magnetic field problem, as happen in axial flux magnetic structures [9].

This paper investigates the applicability of selected formulations in FEM models of rotating electrical machines with a superconducting AC stator winding. An Axial Flux PM (AFPM) machine is considered as case study because of its geometrical configuration that seems to be a more promising solution to cope with the strict minimum bending radii of the SC tapes [10]. To limit the simulation time due to the SC modeling in 3D FEM, a single-slot 2D model is also proposed for time-efficient analyses of SCs during the machine operation.

II. Modeling and Simulation of Superconducting Tapes

Based on the critical temperature, SCs are categorized by the temperature at which the normal to superconducting state transition occurs. They can be low-temperature SCs (e.g. NbTi, T_c=9.6 K) or high-temperature SCs (such as the BSCCO2223, T_c=110 K or the REBCO with T_c=119 K) [11], [12].

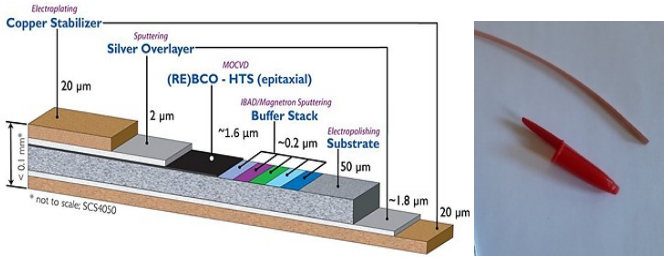

Fig. 1: Sketch of a coated SC REBCO tape (left), and the purchased one (right).

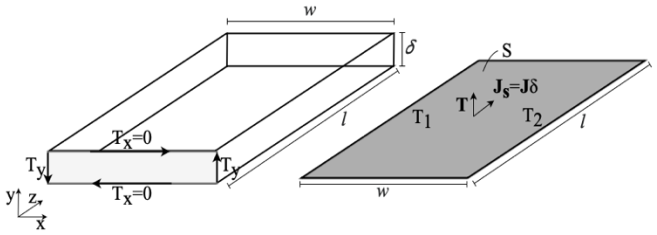

(a) (b)

Fig. 2: Sketch of a SC tape with the modeling variables (a), and the 3D thin-sheet approximation (b).

In the present study, a 4 mm width coated REBCO (Rare Earth Barium Copper Oxide) tape has been considered. As sketched in Fig 1, the superconducting layer has a thickness of 1.6 µm [15]. Figure 1 also depicts on the right side a portion of the tape tested for the calibration of the developed FEM models.

Even if SCs have negligible resistance and, consequently, negligible Joule losses, there could be energy losses inside them. In fact, during the superconductive state and under AC regime, the time-varying magnetic field and currents originate in the SC energy dissipation in the form of heat, known as hysteretic loss [13]. These losses are comparable to the well-known hysteresis losses that occur in magnetic cores, but they are localized in the conductor. The hysteretic losses can be qualitatively explained as the delay in the rotation of magnetic dipoles (i.e. fluxoids) in the penetration zone of the imposed AC current. A more rigorous explanation can be approached referring to the quantum nature of the superconductor physics [14].

A. The T-A formulation

All the formulations reported in the literature for modeling SCs are based on the Maxwell equations, and they are distinguished by the used state variables [12]. This study uses the *T-A* formulation to simulate the SC since it provides a time-efficient method to predict AC losses [16]. In fact, despite SCs have several layers, this formulation allows approximating them to a superconducting surface, significantly reducing the model's computational complexity. This modeling approach is also known as the thin-sheet approximation.

In the superconducting surfaces, the critical current density dependency on the applied magnetic field is imposed by implementing the Kim model in (1), where J_{c0} is the critical current density at B=0T, and B_0 is the magnetic flux density that brings the critical current density to half [17].

$$J_c(\mathbf{B}) = \frac{J_{c0}}{1+|\mathbf{B}|/B_0} \tag{1}$$

The value of J_{c0} can be computed as I_{c0}/S, where I_{c0} is the (critical) current of the superconductor at B=0T and S is the superconducting layer cross-section. Both the value of B_0 and I_{c0} are determined by means of experimental tests on the SC tape.

The non-linear relation between the current and the electric field in SCs can be described by the *E-J* power law in (2) [17].

$$\mathbf{E} = \rho_{SC}\mathbf{J} = E_0 \left(\frac{|\mathbf{J}|}{J_c(\mathbf{B})}\right)^{n-1} \mathbf{J}/J_c(\mathbf{B}) \tag{2}$$

In (2), E_0 is the (critical) electric field, defined as 10^{-4} Vm^{-1} for superconducting tapes, and it is used to measure the SC critical current, while n is the superconducting exponential constant. From (1) and (2), it can be observed that if the magnetic field **B** applied to the SC increases, the critical current density J_c reduces, and consequently the tape quenching risk increases.

For the used SCs tape, the model parameters have been experimentally calibrated [18]. In particular, at 77K, the critical current measured by the DC supply test is 162A, while the B_0=0.140T and n=21 have been extrapolated by measuring the AC losses on the tape.

B. The 3D thin-sheet approximation

Superconducting tapes can be modeled in FEM using the thin-sheet approximation. As Fig. 2 sketches, the thin-sheet approximation considers the tape as a superconducting surface. In 3D, the potential vector **T** is a two-dimensional vector set in the normal direction of the tape's surface. Therefore, to impose a total current I into the tape, two Dirichlet boundary conditions ($T_1 = 0$ and $T_2 = I/\delta$, being δ the SC thickness) are defined along the tape boundaries, as depicted in Fig. 2.b.

Finally, the average AC losses per unit length of the tape (P_{ac}) can be computed by means of (3), where the instantaneous power $p(t)$ is obtained from the FEM model and S is the tape surface area highlighted in gray in Fig. 2.b.

$$p(t) = \frac{1}{l}\iint_S \boldsymbol{E}\cdot(\boldsymbol{J}\delta)\,dS, \quad P_{ac} = \frac{1}{T}\int_0^T p(t)dt \tag{3}$$

Note that the losses computed by (3) account for the hysteretic losses of superconductors when the current is lower than its critical value, and the conductive losses if the current is higher than the critical one.

III. Baseline and Superconducting 3D Machine Models

The considered AFPM machine has been designed by the authors using conventional sizing equations. Figure 3 shows the machine geometry, while Table I lists its main data. Note that neither the design nor the geometry optimization are in the focus of this research activity. Hence, the machine must be considered as a generic and not optimized design solution suitable to apply the SC windings modeling within a '*real*' magnetic circuit. Besides, for the considered speed range of 1000-2000 rpm, 4 poles were chosen to keep low the machine supply frequency.

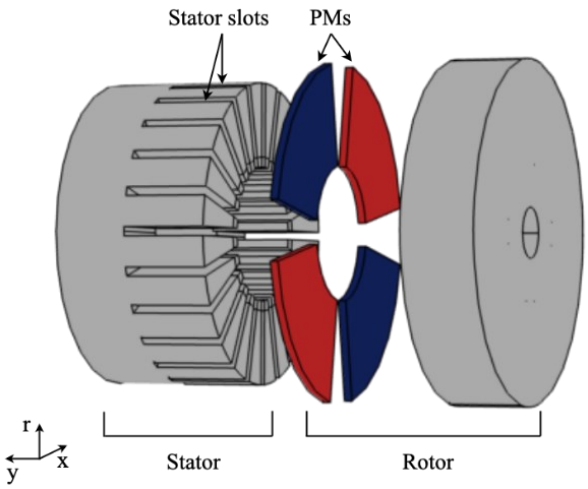

Fig. 3: Axial Flux PM machine geometry considered as case study.

TABLE I. AFPM MAIN DATA

Rated torque (Nm)	95
Rated speed (rpm)	1500
Magnet thickness (mm)	8
Magnet Br, (T)	1.1
Magnet polar pitch, (%)	0.778
Airgap thickness (mm)	1
Outer diameter, (mm)	340
Inner diameter, (mm)	135
Total axial length (mm)	390

In fact, the thin-sheet approximation that models the coated conductor as a superconducting surface has been proved in literature to be successfully applicable for frequencies up to 100 Hz [19].

The study presented in this paper is based on the initial simulation of the AFPM machine equipped with a conventional distributed stator copper winding. The FEM results for this baseline machine are then considered as the reference performance for the second FEM model. The second model is constituted by the same geometry and magneto-motive force as the baseline one, but with the copper conductors of a single slot substituted with SCs – see Fig. 4. This modeling approach has been adopted since considering superconducting elements for all the stator slots would have been extremely complex and unpracticable, both from the model implementation and the resolution time viewpoints.

To further reduce the model complexity the end-windings are not modeled, and proper boundary conditions are imposed on each conducting element to assure the correct winding distribution. Assuming an even subdivision of the rated slot current of 810A, nine tapes per slot were selected for the considered AFPM machine. In this way, the transport current in each SC results well below the critical current of the considered REBCO tape (i.e., 90A per conductor, which is approximately 55% of the critical current) [15]. For the sake of modeling simplification, the same number of tapes per slot has also been considered for the copper conductors. This would obviously be impracticable for a prototype because of the much lower current density capability of the copper windings compared to SCs.

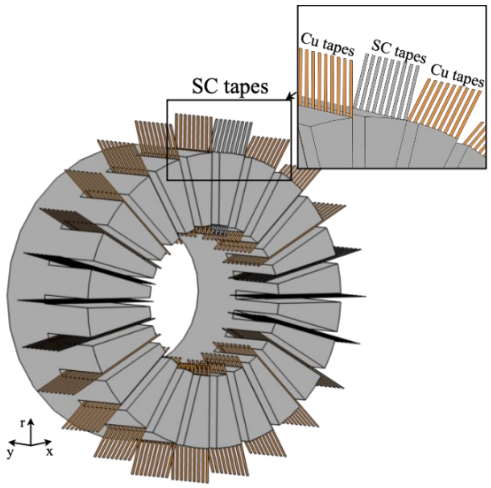

Fig. 4: SC-AFPM machine stator with SCs in one slot (gray) and copper tapes on remaining slots (orange).

However, this simplification can be considered acceptable since the target of this work is on the SC modeling approach and not on the machine performance assessment. Moreover, also the skin effect on the copper conductors was not modeled at this study stage.

Since the simulations are solved imposing the stator current on the machine winding, no limitations on the supply voltage have been considered. The developed 3D FEM model with SCs in one slot is solved in '*only*' tens of hours using a standard desktop computer with 32GB of RAM.

IV. RESULTS FOR THE 3D FEM MODELS

Figure 5 shows the air gap magnetic induction and the electromagnetic torque for the 3D FEM model with stator copper windings (Cu-AFPM) and for the same model with SCs in one slot (SC-AFPM). The models take into account a SiFe magnetizing curve measured at cryogenic temperatures, as well as the calibrated SC tape model [20].

The simulations are performed imposing a sinusoidal current in the *q*-axis only. Being the imposed stator current the same for Cu-AFPM and SC-AFPM models, the air gap magnetic induction and the electromagnetic torque are expected to be the same. The slight difference between the obtained air gap field waveforms is due to the dense mesh used to analyze the superconducting machine. It is also worth noting that when SCs are modeled, a step function in the PMs remanent field and stator currents is imposed in the beginning of the simulation to improve the SC model convergence. For this reason, the results in Fig. 5.b are shown starting at t = 0.02s.

Simulations demonstrate that either the model with all copper conductors and the one having SCs into one slot provide the same results in terms of air gap magnetic induction and electromagnetic torque. It is nevertheless important to highlight that the power losses at the copper or superconducting windings are very different. The obtained results prove the appropriateness of the proposed modeling approach to analyze the behavior of electrical machines equipped with SCs.

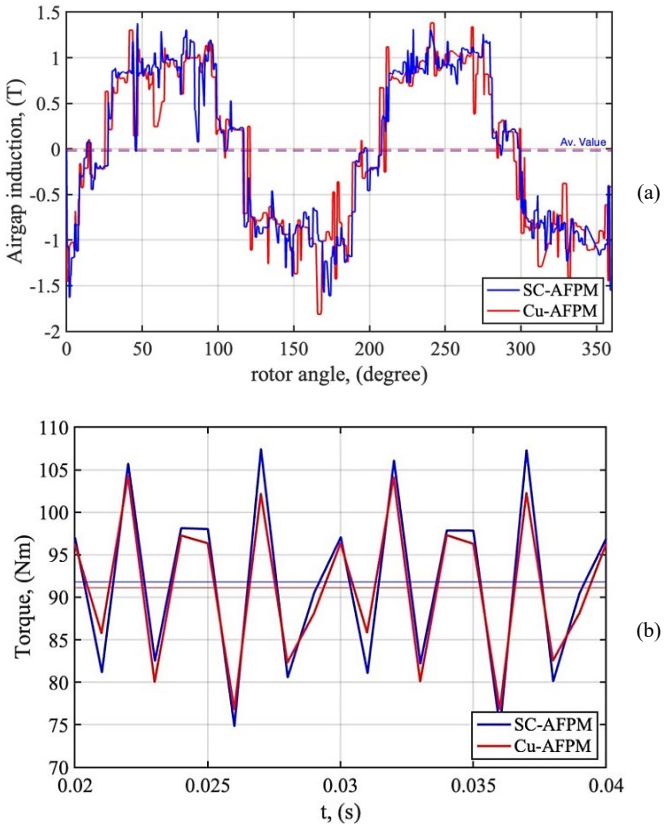

Fig. 5: Air gap magnetic induction (a) and electromagnetic torque (b) for the 3D FEM models with stator copper windings and with SC tapes in one slot.

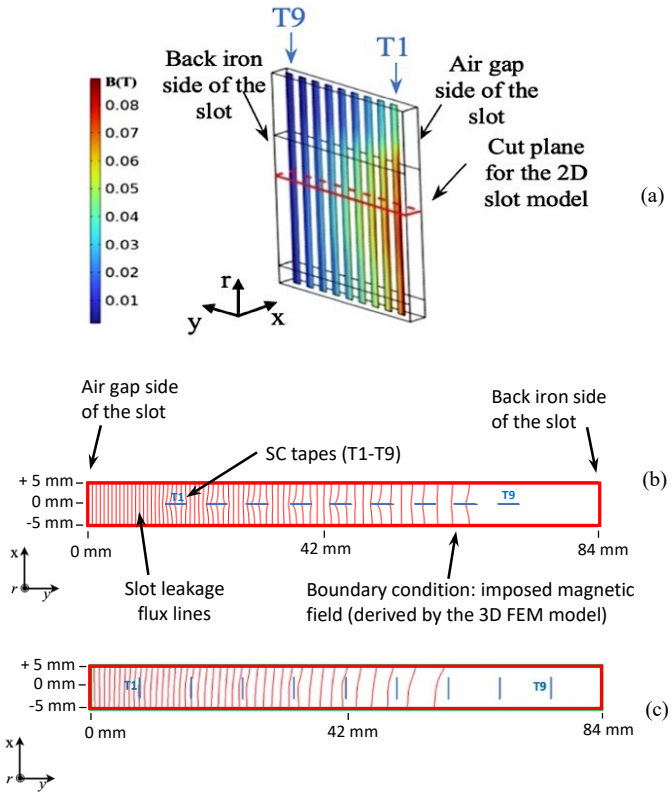

Fig. 6: Magnetic flux density on the surfaces of the SC tapes T1-T9 (a) and the 2D single-slot model for different tape orientations: parallel ∥ (b) and perpendicular ⊥ (c) to the slot *y*-axis.

V. 2D FEM Model of a Single-Slot

Depending on the positioning into the slot, the SCs can be subjected to different amplitudes of leakage magnetic field. Being impossible to investigate different design solutions with 3D FEM simulations of the complete superconducting winding, the authors propose a simplified single-slot 2D FEM model to perform straightforward and time-efficient FEM analyses on the SCs' behavior while still considering the electrical machine operations. With the proposed approach, the simulation time for the 2D single-slot model is reduced to a few minutes only.

As for the tridimensional model, also for the 2D model the *T-A* formulation described in Section II has been applied. In the 2D model, the thin-sheet approximation of the superconducting tape corresponds to a line. Hence, the potential vector **T** is defined in the *y* or *x*-direction (depending on the tape's orientation – see Fig. 6) on the two tape edges. Also in this case, the total current *I* in the conductor is imposed by means of two Dirichlet boundary conditions on these edges.

For the 2D thin-sheet approximation, the average AC tape losses per unit length can be computed using (4), where *w* is the tape width.

$$p(t) = \int_w \boldsymbol{E} \cdot (\boldsymbol{J}\delta)\, dw, \quad P_{ac} = \frac{1}{T}\int_0^T p(t)dt \qquad (4)$$

As for the 3D FEM model, also in this case (4) considers the hysteretic losses and the conductive losses of the SC depending on the current amplitude with respect to the critical current value.

A. Boundary conditions for the 2D model

The magnetic field into the slot of a PM electrical machines is due to the conductors' self-field (i.e., the well-known slot leakage magnetic field), plus the magnetic field generated by the permanent magnets. For the considered AFPM case study, this second contribution is significant because of the thin width of slots designed to host very small SCs. In the single-slot 2D FEM model, the rotating magnetic field due to the permanent magnets is imposed by means of boundary conditions derived by the 3D model, as sketched in Fig. 6. For this purpose, the 3D machine model was initially simulated with null stator current to analyze only the PMs rotating field.

The magnitude of the slot leakage field was evaluated at different slot radial coordinates (*r* direction in Fig. 6.a). Nonetheless, it was verified that the flux density presents limited variations along the slot radial direction at any *y*-axis coordinate. Hence, a cut plane at the middle of the slot height was considered for the boundary magnetic field strength analysis (indicated by a rectangular cut plane with red borders in Fig. 6.a). For a specific time instant when the considered slot is affected by the maximum flux produced by the permanent magnets and without stator currents, Fig. 7.a shows that on the red border of the identified cut plane the B_x component varies linearly along the slot depth (*y*-axis), with the maximum magnitude observed at the air gap border and the lowest magnitude at the back iron border. Consequently, B_x is applied in the 2D model by linear interpolated relation between the values at each border.

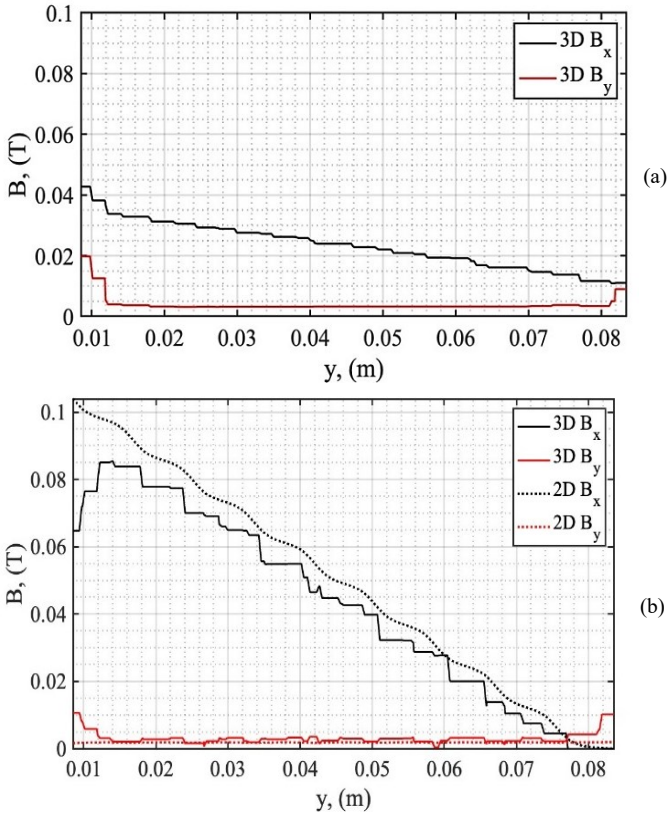

Fig. 7: Flux density components along the x and y directions by the 3D FEM without current (a), and by the 3D and 2D FEM with current (b). Field evaluated in the y direction on the red border of the cut plane in Fig. 6.a.

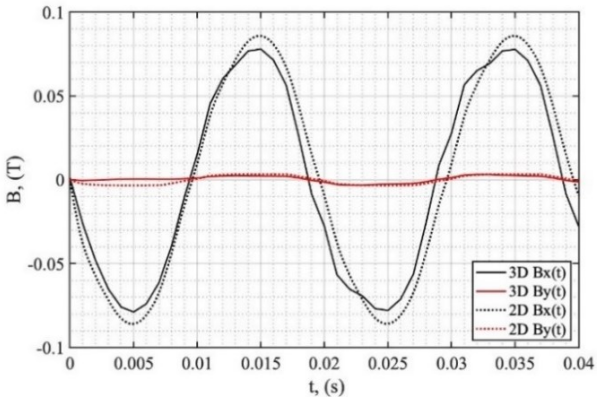

Fig. 8: Time evolution of the magnetic field at y= 0.02 m during two 3D and 2D simulation cycles.

In contrast, the B_y component demonstrated minimal variation along the y-axis. Hence, it was approximated as a constant value along the slot depth. Furthermore, to account for the time dependence of the machine rotating field, in the 2D model the B_x and B_y boundary conditions are applied as a time-dependent function of the magnetic field, $B(t)=B_{x,y}\sin(\omega t+\theta)$, where θ is the phase difference between the slot current and the rotating field. In the case of the simultaneous presence of the maximum current in the SCs and the maximum permanent magnetic flux that flow through the slot (i.e. a worst operative condition for the SC), Fig. 7.b shows the B_x and B_y for the 2D simulation. In the same figure, the results of the 3D model for current control in q-axis are included for completeness.

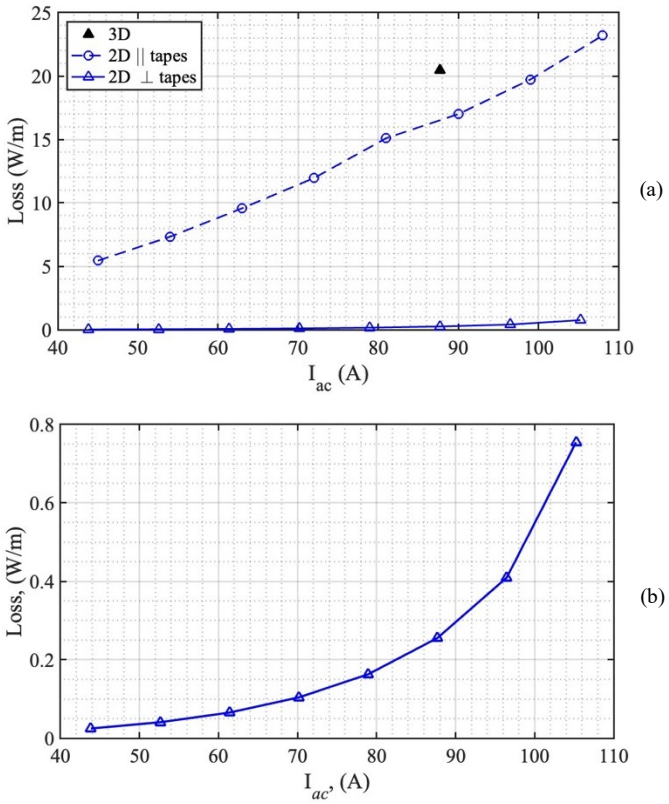

Fig. 9: Losses on the SCs by the 3D FEM and by the 2D single-slot model for two different tapes orientation (a), and zoom for the 2D ⊥ tapes (b).

Since the proposed single-slot 2D modelling approach significantly reduces the computational time, it allows imposing a much finer mesh compared to 3D model. Therefore, the results in Fig. 7.b vary more smoothly for the 2D model than those for the 3D. Figure 8 shows the time evolution for the B_x and B_y flux density components at the slot depth $y=0.02$ m. Also in this case, a good match between the 3D and 2D waveforms is obtained, despite a small phase shift between the 3D FEM and 2D FEM models has been observed.

B. Example of application of the single-slot 2D FEM model

As the literature reports, the magnetic field strength that invest the SC tape perpendicularly has the most critical contribution in increasing the losses, while a magnetic field parallel to the tape has the lowest influence [21]. Even though this is true for SC tapes in general, the model in (2) only considers the magnitude of **B** instead of different weights for perpendicular and parallel components (to the tape's widest surface). Nonetheless, by using the thin-sheet approximation, the induced current loops in the superconductor layer will be maximum when the magnetic field is perpendicular to the tape's wide surface.

As Fig. 7 shows, the field contribution inside the slot is mainly in the x-axis direction. Therefore, it is proposed here a 90º rotation for the tapes, as shown in Fig. 6.c, to study the effect of the relative tapes' orientation on their losses. Analysis of the field on the machines with 90º rotated tapes (i.e. ⊥ tapes) allowed to verify that the field at the slot boundaries is the same as for the previous tapes' orientation.

Figure 9 reports the losses estimated in the SCs by the 3D FEM model with SCs in one slot, and by the single-slot 2D FEM model with the SC tape oriented as in Fig. 6.b and oriented as in Fig. 6.c. Note that in Fig. 9 the results for the 3D FEM model are shown only for the machine rated operation point because of the large computational time required by the 3D simulation to compute the SC losses. The results show that the single-slot 2D FEM model well agrees with the 3D results, validating the proposed modeling approach.

It should be noticed that Fig. 9.a shows a limit condition where the SC tapes oriented parallelly to the slot *y*-axis quench. In this case, the winding losses are approximately comparable with those of a conventional copper winding in cryogenic conditions, neglecting the skin effect. This proves that the use of the SC tapes with the parallel positioning is only not possible from the quenching point of view, but also because it seems to not provide a real benefit with respect to a conventional copper winding machine at cryogenic temperatures.

Nonetheless, the FEM simulations demonstrated that the perpendicular positioning of the superconducting tapes prevents the quenching risk providing minimal losses per unit length – see Fig. 9.b. This finding agrees with the conclusion provided in [21]. By the way, the perpendicular conductor's orientation in the slot makes possible the realization of toroidal winding solutions that better allow respecting the minimum bending radii of commercial superconducting tapes and the use of multistage AFPM machines.

VI. Conclusion

The paper presents the formulations for modeling SC tapes in FEM simulations suitable for rotating electrical machines. A calibrated SC tape model has been successfully applied for the AC winding of a hypothetical AFPM machine design, investigated by means of 3D FEM models due to its tridimensional nature of the magnetic field problems. Consequently, a single-slot 2D FEM model has been proposed for time-efficient simulations that allows investigating different tape positioning in the slot.

The study confirms that the applicability of SCs tapes with AC supply could be critical and requires special care since from the design stage. In particular, it was found that the perpendicular orientation of the tape in the slot makes possible the adoption of SCs for AC windings of rotating electrical machines.

Acknowledgments

The research activities developed by Inês S. P. Peixoto have been conducted in the frame of the Doctoral Research programme funded by the Italian Ministry of University and Research through the Operative National Program (PON) for Research and Innovation 2014-2020, M.D. 1061 (10 Aug. 2021), Action IV.5 "Ph.D. programmes on sustainability-based topics".

References

[1] K.S. Haran, S. Kalsi, T. Arndt, et al., "High power density superconducting rotating machines—development status and technology roadmap," *Superconductor Science and Technology*, vol. 30, no. 12, p. 123002, Nov. 2017.

[2] C.C.T. Chow, M.D. Ainslie, K.T. Chau, "High-temperature superconducting rotating electrical machines: An overview," *Energy Reports*, vol. 9, pp. 1124-1156, 2023.

[3] I. Marino, A. Pujana, G. Sarmiento, S. Sanz, J. M. Merino, M. Tropeano, J. Sun, and T. Canosa, "Lightweight mgb2 superconducting 10 mw wind generator," *Superconductor Science and Technology*, vol. 29, no. 2, 2015.

[4] C. A. Luongo, P. J. Masson, T. Nam, D. Mavris, H. D. Kim, G. V. Brown, M. Waters, and D. Hall, "Next generation more-electric aircraft: A potential application for hts superconductors," *IEEE Trans. Applied Supercond.*, vol. 19, no. 3, pp.1055–1068, 2009.

[5] F. Weng, M. Zhang, T. Lan, Y. Wang and W. Yuan,"Fully superconducting machine for electric aircraft propulsion: stufy of AC loss for HTS stator", *Supercond. Sci. Technol.*, vol. 33, no. 10, 2020.

[6] T. Nakamura et al., "Load Test and Variable Speed Control of a 50-kW-Class Fully Superconducting Induction/Synchronous Motor for Transportation Equipment," *IEEE Trans. Applied Supercond.*, vol. 29, no. 5, pp. 1-5, Aug. 2019.

[7] T. Qu et at, "Development and testing of a 2.5 kW synchronous generator with a high temperature superconducting stator and permanent magnet rotor," *Supercond. Sci. Technol.*, vol. 27, no. 4, 2014.

[8] K. Kovalev, N. Ivanov, S. Zhuravlev, Ju Nekrasova, D. Rusanov and G. Kuznetsov, "Development and testing of 10 kW fully HTS generator", Journal of Physics: Conference Series, 14th European Conf. Appl. Supercond., Glasgow, UK, vol. 1559, September 2019.

[9] Y. Statra, H. Menana, B. Douine, "3D Semi-Analytical Modeling and Optimization of Fully HTS Ironless Axial Flux Electrical Machines," Physica C: Superconductivity and its Applications, vol. 574, 2020.

[10] G. De Donato, F. Giulii Capponi, F. Caricchi, "Fractional-slot concentrated-winding axial-flux permanent-magnet machine with core-wound coils," *IEEE Trans. Ind. Appl.*, vol. 48, no. 2, pp. 630–641, 2012.

[11] D.U. Gubser, "Superconductivity: an emerging power-dense energy-efficient technology," *IEEE Trans. Appl. Supercond.*, vol. 14, no. 4, pp. 2037-2046, Dec. 2004.

[12] Z. Hongye, Z. Wen, F. Grilli, K. Gyftakis, and M. Mueller, "Alternating Current Loss of Superconductors Applied to Superconducting Electrical Machines" *Energies,* vol.14, no. 8: 2234, 2021.

[13] F Gömöry et al., "Predicting AC loss in practical superconductors," *Supercond. Sci. Technol.*, vol. 19, no. 3, pp. S60-S66, 2006

[14] C.M. Rey, A.P. Malozemoff, "Superconductors in the Power Grid - Fundamentals of superconductivity", Woodhead Publishing, 2015, pp. 29-73.

[15] SuperPower Inc., [Online]. Available: http://www.superpower-inc.com

[16] F. Huber, W. Sohng, M. Zhang, F. Grilli, "The t-a formulation: an efficient approach to model the macroscopic electromagnetic behaviour of hts coated conductor applications," *Supercond. Sci. Technol.*, vol. 35, no.4, Mar. 2022.

[17] Z. Jiang et al., "AC Loss Characteristics of YBCO Coated Conductors With Varying Magnitude of Critical Current," *IEEE Trans. Applied Supercond.*, vol. 16, no. 2, pp. 85-88, June 2006.

[18] J. Zhu, Z. Zhang, H. Zhang, M. Zhang, M. Qiu and W. Yuan, "Electric Measurement of the Critical Current, AC Loss, and Current Distribution of a Prototype HTS Cable," *IEEE Trans. Appl. Supercond.*, vol. 24, no. 3, June 2014, Art no. 9500104.

[19] H. Zhang et al., "Modelling of electromagnetic loss in HTS coated conductors over a wide frequency band," *Supercond. Sci. Technol.*, vol. 33, no. 2, 2020, pp. 025004.

[20] M. Biasion, I.S.P. Peixoto, J.F.P. Fernandes, S. Vaschetto, G. Bramerdorfer and A. Cavagnino, "Iron Loss Characterization in Laminated Cores at Room and Liquid Nitrogen Temperature," Conf. Rec. IEEE-ECCE, Detroit, MI, USA, 2022, pp. 1-8.

[21] N. Amemiya, Z. Jiang, Y. Iijima, K. Kakimoto, and T. Saitoh, "Total AC loss of YBCO coated conductor carrying AC transport current in AC transverse magnetic field with various orientations," *Supercond. Sci. Technol.*, vol. 17, pp. 983–988, 2004.